

# A brief introduction to fluctuation theorems: from theory to experiments

Thalyta T. Martins<sup>1,\*</sup>, André H. A. Malavazi<sup>2,†</sup>, Lucas P. Kamizaki<sup>1,3</sup>, Artyom Petrosyan<sup>4</sup>, Benjamin Besga<sup>5</sup>, Sergio Ciliberto<sup>4</sup>, and Sérgio R. Muniz<sup>1,‡</sup>

<sup>1</sup>*Instituto de Física de São Carlos, Universidade de São Paulo, 13560-970 São Carlos, SP, Brazil*

<sup>2</sup>*International Centre for Theory of Quantum Technologies,*

*University of Gdańsk, Jana Bażyńskiego 1A, 80-309 Gdańsk, Poland*

<sup>3</sup>*Instituto de Física ‘Gleb Wataghin’, Universidade Estadual de Campinas, 13083-859 Campinas, SP, Brazil*

<sup>4</sup>*Université de Lyon, ENS de Lyon, CNRS, Laboratoire de Physique, F-69342 Lyon, France*

<sup>5</sup>*Universite Claude Bernard Lyon 1, CNRS, institut Lumière Matière, UMR 5306, F69100 Villeurbanne, France*

(Dated: March 28, 2025)

Thermodynamics is a fundamental branch of physics, and over the years, it has evolved to include mesoscopic and out-of-equilibrium systems driven by theoretical and experimental advances at the micro- and nanoscale. This development has led to *stochastic thermodynamics*, a framework that connects microscopic fluctuations with macroscopic laws. Despite their significance, fundamental ideas, such as fluctuation theorems, are frequently not covered in current curricula, leaving them largely unknown across many disciplines. Here, we present the core results of stochastic thermodynamics, particularly the Jarzynski equality and the Crooks theorem, using an integrated approach combining theoretical foundations with experimental verification using optical tweezers. This approach helps to clarify the fundamentals, linking theoretical ideas to real elements in the lab, showing the simplicity of the apparatus, and presenting detailed procedures for calibration and calculation of relevant quantities to enable the implementation of these experiments in new research and teaching laboratories. The goal is to enrich thermodynamics education and to stimulate exploration in this evolving field.

## I. INTRODUCTION

Thermodynamics is one of the most important and well-established physical theories [1–3], with wide use and an impressive range of applications in other disciplines, especially chemistry and engineering. Despite the initial pragmatic approach, it succeeded in not just surviving contemporary advancements but thriving and attaining a prominent position thanks to the effective universality of its statements. In this sense, the laws of thermodynamics proved to be a solid basis for understanding nature, with direct applications ranging from biology [4] to black hole physics [5–7].

The early discipline of thermodynamics was restricted to describing macroscopic *systems in equilibrium* and *quasistatic processes*. Thermodynamic equilibrium refers to static (time-invariant) states of macroscopic variables such as volume, pressure, and temperature. Quasistatic processes are idealized transformations in which the system is maintained in equilibrium throughout its evolution. Another central concept is the notion of reversibility, which assures that the system can be returned to a previous state by reverting some relevant parameters. This is intrinsically related to the condition of quasistatic transformations. For these conditions to hold, quasistatic processes must proceed very slowly because quick shifts in the system’s configuration could push it out of equilibrium. However, in truly macroscopic systems, equilibration usually happens quickly enough to treat finite-time changes as approximately quasistatic. Notice that despite the term *thermodynamics*, the foundational equilibrium theory does not portray dynamic processes in the usual sense. The dynamics

are given through relations between macroscopic quantities, but the underlying evolution remains hidden. Thus, while effectively predicting a system’s final state, the theory lacks the tools to describe *how*, *at what rate*, or *through which mechanisms* a system transitions to equilibrium. Capturing these dynamic aspects usually requires other frameworks to describe the connection to the underlying microscopic processes.

The advent of statistical physics started to bridge the gap with the microscopic nature of matter [8]. This progress introduced probabilistic and statistical reasoning, which proved highly successful in describing microscale physics and justifying previous phenomenological observations. Good examples are Einstein’s explanation of Brownian motion and Perrin’s confirmation of the atomic hypothesis [9, 10]. These developments paved the way for extending the theory to consider smaller systems far from equilibrium, including finite-time protocols. Under these circumstances, fluctuations become non-negligible and play a significant role in the physical description. These advancements are now contained within the broader context of *stochastic thermodynamics* [11–13], which provides a general framework to define quantities such as work, heat, and entropy, for mesoscopic systems following trajectories in phase space. In this context, these quantities are understood as dynamic stochastic variables that can acquire different values for distinct process realizations, and familiar laws of thermodynamics are recovered at the average level over an *ensemble* of realizations.

The fluctuation theorems (FTs) encapsulate some of the most important results of the field [14–22]. Among them, the most well-known were proposed by Jarzynski [23] and Crooks [24] regarding non-equilibrium work relations. In essence, FTs offer general mathematical statements for the probability distribution of relevant thermodynamic quantities. It is fascinating how these simple relations carry profound conceptual meanings and far-reaching consequences despite

\* thalyta.tavares.martins@gmail.com

† andrehamalavazi@gmail.com

‡ srmuniz@ifsc.usp.br

their straightforward structures. Experimentally, they are well established and verified across numerous platforms [25, 26], such as electrical circuits [27], mechanical torsion pendulums [28], and single-electron boxes [29] (see, for instance, [30]). Furthermore, these results have been extended to the quantum regime [31–36], in quantum thermodynamics [37–39], and also experimentally verified in various settings [30].

Among the experimental platforms, optical tweezers were the first to be used and still are one of the most versatile and widely employed. Optical tweezers (OTs) are powerful tools for probing and verifying physical phenomena at the micro-scale [40]. These devices use focused laser beams to trap microscopic systems in a non-invasive manner [41]. Using it, researchers can control and analyze systems with a high spatial and temporal resolution by tailoring optical potentials [40]. The setup is relatively simple, requiring only standard optical components. The precision and simplicity of OTs make optically trapped particles ideal testbeds for experimentally assessing stochastic thermodynamics. Optical trapping has been used in numerous studies to explore these scales [42–49]. For a comprehensive review, see [50].

Despite the importance and significant progress in stochastic thermodynamics over the past decades, key concepts and main results remain underrepresented in the standard education of physicists and other fields, which makes this knowledge not widely diffused among students and active researchers. To help address this gap, updating thermodynamics curricula with verifiable experiments, this paper aims to contribute to this effort by introducing the main results of stochastic thermodynamics in a clear, accessible manner for undergraduate students and new researchers. Additionally, we explain how optical setups can be used to probe non-equilibrium thermodynamics quantities at the mesoscopic scale. Since it can be easily implemented, this work may also help set up experimental courses and new research labs in related fields.

This paper is structured in two main parts: Section II presents the foundations, starting with a brief overview of macroscopic thermodynamics and introducing stochastic thermodynamics and fluctuation theorems. It then describes the use of optical tweezers to study the thermodynamics of mesoscopic systems. Section III details the experimental setup, data acquisition and calibration methods, results, and analysis. Finally, Section IV provides the discussion and conclusions.

## II. THEORY

This section outlines the necessary theoretical foundations. It begins with a quick outline of the first and second laws, establishing the basic concepts and terminology. Next, it introduces the fundamental non-equilibrium work relations, expressed by the Jarzynski Equality and the Crooks Fluctuation Theorem, while providing the basic framework and notation of stochastic thermodynamics needed to understand the analysis in the following sections.

### A. Fundamentals of Equilibrium Thermodynamics

The *first law of thermodynamics* states the principle of energy conservation, distinguishing between two forms of energy change: work ( $W$ ) and heat ( $Q$ ). For a given thermodynamic system undergoing an arbitrary process  $\Gamma$ , the infinitesimal change in internal energy  $dU$  is given by [2]:

$$dU = \delta W + \delta Q, \quad (1)$$

where  $\delta W$  and  $\delta Q$  represent inexact differentials and highlight that these quantities are not state functions, indicating that they depend on the path  $\Gamma$ . In addition, they are fundamentally distinct. Work ( $W$ ) represents energy exchanged due to changes in external variables (e.g., volume), usually acted by an external agent, while heat ( $Q$ ) is energy transferred primarily due to temperature gradients between systems in thermal contact, although this can occur through various mechanisms like conduction, convection, or radiation.

The *second law of thermodynamics* introduces the concept of entropy ( $S$ ) and addresses the feasibility and reversibility of processes. Essentially, it constrains conceivable processes even more, limiting even those satisfying the first law. For a system in contact with a thermal bath at temperature  $T$ , it can be expressed as [2]:

$$dS \geq \frac{\delta Q}{T}, \quad (2)$$

with equality holding only for reversible processes. In the case of an isolated system, where no heat exchange occurs, the second law simplifies to  $dS \geq 0$ . For irreversible processes, the system moves towards non-equilibrium, and the entropy change is strictly positive.

Equations (1) and (2) are entirely general and can be adapted to more convenient variables by introducing thermodynamic potentials via Legendre transformations. For example, the Helmholtz free energy, defined as  $F := U - TS$ , allows the second law to be reformulated for isothermal (constant temperature) processes as:

$$\delta W \geq dF. \quad (3)$$

This form indicates that the minimum (or maximum) work performed (or received) is bounded by the change in free energy between the initial and final equilibrium states, with equality holding only for reversible processes.

### B. Brief Overview of Stochastic Thermodynamics

Equilibrium thermodynamics normally ignores fluctuations in macroscopic systems for good reasons. As an illustration, consider a 3D box filled with an ideal monoatomic gas of  $N$  particles in thermal equilibrium at temperature  $T$ . The equipartition theorem gives the average internal energy  $\langle U \rangle_T = \frac{3}{2} N k_B T$ , where  $\langle \cdot \rangle_T$  represents averages over equilibrium quantities, and  $k_B$  is the Boltzmann constant. The variance of the energy is given by  $\text{Var}(U) = \frac{3}{2} N k_B^2 T^2$ , and the relative fluctuation in the internal energy,  $\frac{\sigma_U}{\langle U \rangle_T} = \frac{\sqrt{\text{Var}(U)}}{\langle U \rangle_T} \approx \frac{1}{\sqrt{N}}$ .

This relative fluctuation is negligible for a macroscopic system with  $N \approx 10^{23}$ , and the energy distribution is sharply peaked around its mean value. Allowing fluctuations to be safely ignored in such systems. However, this is no longer true for small systems, say  $N \approx 10^2$ , when fluctuations become significant compared to the relevant energy scales, requiring it to be included in the thermodynamic description.

Let us consider another illustrative example with a thought experiment where a box undergoes repeated cycles of the *same* protocol, such as an isothermal expansion that doubles its volume. In a macroscopic box, where the number of particles is large, fluctuations in pressure and volume due to particle collisions with the walls are negligible. Consequently, the uncertainty in the measured average work is much smaller than the mean work value.

In contrast, if the same experiment is performed in a microscopically sized box with a small number of particles, the relative fluctuations in pressure become significant, even in an idealized hard-wall box. This leads to noticeable fluctuations in the measured average work, even after many repetitions of the protocol and perfect measurements. Fig. 1 illustrates this scenario for mesoscopic systems, where fluctuations are on the order of  $k_B T$ : large enough to be observable but small enough to cause significant measurement deviations.

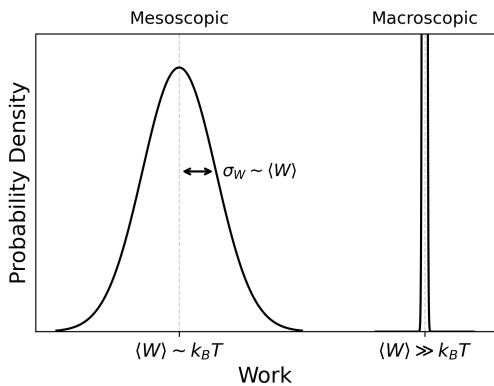


FIG. 1. Work probability density for mesoscopic and macroscopic systems, with average values indicated by dashed lines. Fluctuations are negligible in macroscopic systems, and uncertainty is limited only by measurements, while for mesoscopic systems, fluctuations are significant, with values comparable to the average work  $\langle W \rangle$ .

Stochastic thermodynamics treats quantities like internal energy, work, and heat as stochastic variables, allowing the portrayal of average and individual trajectories in phase space for finite-time processes and non-equilibrium states.

Let  $\mathbf{x} := (\mathbf{q}, \mathbf{p})$  represent the phase-space coordinates for a small system in contact with a thermal bath, and let  $\lambda$  denote an external control parameter (e.g., potential, position, or magnetic field). A modification of  $\lambda$ , parameterized by time  $t$ , defines a *protocol*,  $\lambda(t)$ . Due to the bath's stochastic fluctuations, phase-space trajectories vary even under identical protocols. The Hamiltonian of the system,  $H(\mathbf{x}, \lambda)$ , represents its internal energy  $U(\mathbf{x}, \lambda)$ . Energy changes can arise from shifts in phase space variables (heat,  $Q$ ) or from changes in external parameters (work,  $W$ ), consistent with the first law of thermo-

dynamics:

$$dW := \frac{\partial U}{\partial \lambda} d\lambda, \quad dQ := \frac{\partial U}{\partial \mathbf{x}} d\mathbf{x}. \quad (4)$$

Therefore, given a protocol  $\lambda(t)$ , the total work along a single trajectory over time  $t$  is simply

$$W = \int_0^t \frac{\partial U}{\partial \lambda} \frac{d\lambda}{dt'} dt', \quad (5)$$

with an analogous expression for the heat.

Although it is outside the scope of this introduction, it is worth mentioning that the same reasoning can be applied to define fluctuating entropy [51], for example.

Finally, the ensemble average of work, obtained by repeating the protocol multiple times, is:

$$\langle W \rangle = \int_0^t \left\langle \frac{\partial U}{\partial \lambda} \right\rangle \frac{d\lambda}{dt'} dt' = \int W P(W) dW, \quad (6)$$

where  $P(W)$  is the probability distribution function of work and  $\langle \cdot \rangle$  represents the ensemble average over the realization.

### 1. Brownian motion

The erratic trajectory of a mesoscopic particle immersed in a fluid is well described by the paradigmatic *Brownian motion* [9]. This motion results from collisions with numerous surrounding particles, making it an excellent testbed for the formalism of stochastic thermodynamics.

Let us consider a Brownian particle subjected to a one-dimensional potential  $U(x)$ , initially in thermodynamic equilibrium with its environment (fluid) at temperature  $T$ . The particle's time evolution is fully characterized by the *Langevin equation* [52, 53]:

$$m\ddot{x} = -\gamma\dot{x} - \frac{dU(x)}{dx} + F_{th}, \quad (7)$$

where  $F_{th}$  is the stochastic force, given by Gaussian white noise arising from the system's interaction with its thermal reservoir characterized by:  $\langle F_{th}(t) \rangle = 0$  and  $\langle F_{th}(t) F_{th}(t') \rangle = 2\gamma k_B T \delta(t - t')$ , with  $\delta$  being the Dirac delta function. In Eq. (7),  $m$  is the mass of the particle,  $\gamma = 6\pi\eta R$  denotes the particle's friction coefficient, where  $\eta$  is the medium's viscosity and  $R$  the particle's radius. Thus, the particle's dynamics are governed by the deterministic force from the external potential and the stochastic thermal forces, which are non-negligible at the mesoscopic scale.

Figure 2 shows a simulation [54] of Brownian motion for a water-immersed particle in a harmonic potential  $U(x) = \frac{1}{2}\kappa x^2$  over a time interval of  $\tau = 10$  ms, at the top part. The bottom part of the figure contrasts this behavior over  $\tau = 1$  s for different trap stiffnesses,  $\kappa_1 = 1$  pN/ $\mu\text{m}$ , and  $\kappa_2 = 10\kappa_1$ . Higher values of the force constant  $\kappa$  result in the particle being more spatially constrained, evident from the smaller standard deviation of its center of mass position.

Sekimoto [55] showed that when the particle is subjected to an external control parameter  $\lambda(t)$ , the trajectory can be related

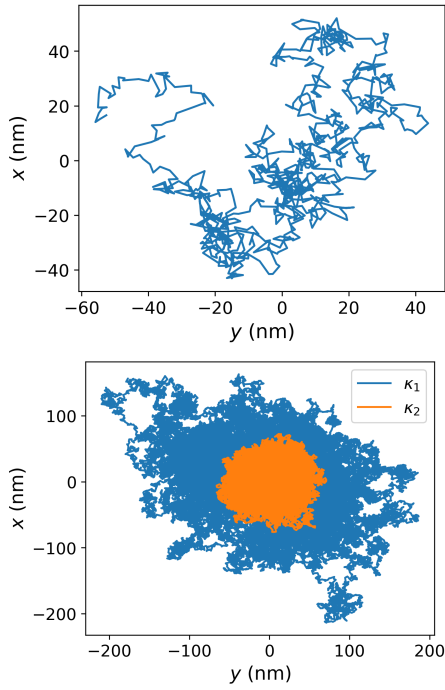


FIG. 2. Simulated trajectories of a water-immersed particle trapped at room temperature in a harmonic potential. (Top) Trajectories for a trap stiffness  $\kappa_1 = 1$  pN/ $\mu\text{m}$  over 10 ms. (Bottom) Comparison of trajectories for trap stiffnesses  $\kappa_1$  and  $\kappa_2 = 10\kappa_1$  over 1 s. The simulations use a time interval of  $10 \mu\text{s}$  between points with parameters:  $T = 300$  K,  $\gamma = 6\pi\eta R$ ,  $\eta = 0.001$  N  $\cdot$  s  $\cdot$  m $^{-2}$ , and  $R = 1 \mu\text{m}$ .

directly to thermodynamic quantities such as heat and work. To establish this connection, consider the overdamped regime of the Langevin equation, where the inertial term is negligible,  $m\ddot{x} \approx 0$ . After rearranging the terms, we obtain:

$$\gamma\dot{x} = -\frac{dU(x)}{dx} + F_{th}(t). \quad (8)$$

According to Sekimoto [55], the heat  $dQ$  exchanged with the thermal reservoir is defined as:

$$dQ = -(-\gamma\dot{x} + F_{th}(t))dx, \quad (9)$$

where the sign convention here is opposite to the usual in macroscopic thermodynamics, therefore  $dQ = -dQ$ .

Using the first law of thermodynamics,  $dU = dQ + dW$ , where  $dW$  is the work done on the system, we can write:

$$dW = dQ + dU = \frac{\partial U}{\partial \lambda} d\lambda. \quad (10)$$

Thus, the stochastic work applied to the system by the external control along the trajectory  $x(t)$  is given by Eq. (5), and the stochastic heat dissipated by the system into the bath is:

$$Q = \int_0^t dt' [(-\gamma\dot{x} + F_{th}(t'))\dot{x}]. \quad (11)$$

Therefore, from the particle's trajectory  $x(t)$  and values of the control parameter  $\lambda(t)$  of the modulated potential, it is possible

to compute the time evolution of work and heat during a given (single) process and determine their final values using Eq. (5) and Eq. (11). Because of the stochastic force, each realization will result in different values, and one can obtain their average across an ensemble of trajectories, as in Eq. (6).

For completeness, one might be interested in an ensemble-level description of this physical setting instead of the individual trajectory picture provided by the Langevin equation. This is captured by the *Fokker-Planck equation* [56], which characterizes the dynamics of the probability density function  $P(x, t)$  corresponding to the particle's position  $x$  at time  $t$ :

$$\frac{\partial P(x, t)}{\partial t} = \frac{1}{\gamma} \frac{\partial}{\partial x} \left[ \frac{dU(x)}{dx} P(x, t) + k_B T \frac{\partial P(x, t)}{\partial x} \right]. \quad (12)$$

### C. Fluctuation theorems

To describe the thermodynamics of mesoscopic systems accurately, one cannot neglect the role played by fluctuations. Surprisingly, these fluctuations carry valuable information. The FTs provide formal mathematical relations expressing certain system symmetries, usually expressed in terms of the probability distribution of some stochastic variable. This is a broad and rich subject, but here, we will focus on two emblematic results that helped spur the entire field. The reader will find a more comprehensive discussion in [57, 58]. Below, we introduce the non-equilibrium work relations [59].

#### 1. Jarzynski equality

One of the most paradigmatic examples of FT is the Jarzynski equality, initially proposed in [23]. It relates non-equilibrium work distribution within a given protocol to the difference in Helmholtz free energy,  $\Delta F$ .

Let us assume our thermodynamic system of interest is described by a Hamiltonian  $H(x, \lambda)$ , where  $\lambda$  represents the external control parameter. Now, consider the following simple procedure: **(i)** Initially, place the system in thermal contact with a reservoir at temperature  $T$ , with  $\lambda$  fixed at  $\lambda_i$ ; **(ii)** After equilibration, modify  $\lambda$  according to some predefined finite-time protocol until it reaches a final value  $\lambda_f$  [60]. During this execution, stochastic work, as quantified by Eq. (5), is performed. After repeating this process several times, one can calculate the statistics for this process. Under these conditions, the following equality holds:

$$\langle e^{-W/k_B T} \rangle = e^{-\Delta F/k_B T}, \quad (13)$$

where  $\Delta F := F_f - F_i$ , with  $F_{i,f}$  being the Helmholtz free energy relative to the equilibrium state characterized by  $\lambda_{i,f}$ .

This expression is surprising for several reasons. First, it is an equality, which contrasts with the usual thermodynamic relation between work and free energy for non-equilibrium processes (Eq. (3)). Additionally, its derivation and validity do *not* depend on the specific protocol or the system's final state, even though the latter strongly depends on the former.

This means that as long the system reaches  $\lambda_f$ , the work protocol can be executed as rapidly as desired, potentially driving the system to states far from equilibrium. Its main relevance is that one can gain access to helpful equilibrium quantities without relying on quasistatic processes by simply collecting work statistics from arbitrary finite-time processes.

Furthermore, applying Jensen's inequality  $\langle e^x \rangle \geq e^{\langle x \rangle}$ , to Eq. (13) it is possible to recover the standard second law statement (Eq. (3)):

$$\langle W \rangle \geq \Delta F. \quad (14)$$

Notice that this inequality refers to the average value of work, indicating that individual stochastic trajectories may eventually exhibit work values below  $\Delta F$ .

## 2. Crooks fluctuation theorem

Following Jarzynski's proposal, Crooks introduced another general equality related to similar quantities in [24].

To understand Crooks's theorem, consider the same basic procedure as before, but now, both ways are needed: forward and backward. Define a *forward-protocol* as a sequence where  $\lambda$  changes from  $\lambda_i$  to  $\lambda_f$ , and a *backward-protocol* as the time-reversed sequence where  $\lambda$  changes from  $\lambda_f$  back to  $\lambda_i$ . In the forward (backward) execution, the system starts in equilibrium according to  $\lambda_{i(f)}$ .

The Crooks fluctuation theorem is expressed as:

$$\frac{P_F(W)}{P_R(-W)} = e^{(W-\Delta F)/k_B T}, \quad (15)$$

where  $P_F(W)$  is the probability of performing the work  $W$  during the execution of the forward protocol, while  $P_R(-W)$  is the probability of attaining the work  $-W$  during the execution of the backward (reverse) protocol.

This expression encodes several essential insights. First, notice that the distributions  $P_F(W)$  and  $P_R(-W)$  coincide exactly when  $W = \Delta F$ . This feature allows the straightforward identification of  $\Delta F$  by simply observing the intersection point of both stochastic work distributions. Additionally, by directly integrating Eq. (15) and using the normalization of the probability distributions  $\int_{-\infty}^{\infty} dW P_R(-W) = 1$ , one can easily derive the Jarzynski equality in Eq. (13).

Thus, the Crooks fluctuation theorem provides a deeper understanding of non-equilibrium processes and connects forward and reverse protocols, reinforcing the fundamental principles of thermodynamics at the mesoscopic scale.

## D. Probing stochastic thermodynamics with optical tweezers

### 1. Optical tweezers

The development of the first laser optical traps began in the late 1960s when Arthur Ashkin observed that a laser beam could push micrometer-sized transparent particles due to radiation pressure. Subsequently, the counter-propagating beam

trap was used to demonstrate the first all-optical trap [61], and years later, the first single-beam trap, known as *optical tweezers*, was introduced [41]. This tool revolutionized the way scientists interact with microscopic objects, mainly due to its ability to precisely manipulate micro and nanoscale systems in a non-invasive manner using forces exerted by light. In fact, due to its numerous applications across various scientific fields, from studying biological systems [62–65] and chemical processes [66] to studies of thermodynamics at the microscale [25, 67, 68], Arthur Ashkin was awarded the 2018 Nobel Prize in Physics for developing this powerful tool.

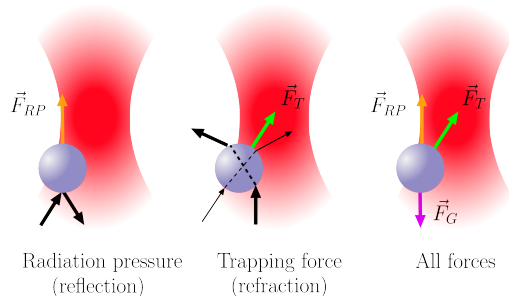


FIG. 3. The basic scheme of the beam's trajectory (black lines) during the reflection and refraction, and the resulting forces are radiation pressure (orange) and trapping force (green), respectively. The gravitational force (purple) is also represented but usually is much smaller.

For the discussion here, focused on stochastic thermodynamics, and given the size of the optically trapped particle (with  $R \approx 1 \mu\text{m}$ ), we can safely use the simplest description for the operation of the optical tweezer, using geometric optics and momentum conservation. For further details and more general descriptions, one can refer to [40, 50, 69].

An optical tweezer employs a highly focused laser beam to manipulate a microscopic particle (Fig. 3). As light reflects and refracts upon entering and exiting the particle, its momentum changes, generating a radiation pressure force ( $\vec{F}_{RP}$ ) along the beam axis and a trapping (gradient) force ( $\vec{F}_T$ ) toward the region of highest intensity at the focal point. For materials with an index of refraction larger than its surroundings, like silica beads in water,  $\vec{F}_T$  is attractive, balancing  $\vec{F}_{RP}$  and the small gravitational force ( $\vec{F}_G$ ) to achieve stable trapping.

The resulting force can be approximated as a linear restoring force for small particle displacements from its equilibrium position, expressed as  $F_{OT} = -\kappa x$ . In this regime, the trapped particle behaves like a mass-spring system in a harmonic potential  $U = \frac{1}{2}\kappa x^2$ , as illustrated in Fig. 5. In addition, it is possible to dynamically control relevant parameters like spring constant  $\kappa$  and the equilibrium position simply by adjusting the beam intensity and position. Moreover, by appropriately controlling temporal and spatial modulations of the beam, a wide variety of optical potentials can be generated [47, 70], making OTs a versatile platform for experimental research.

## 2. Mechanical analogy & control protocols

In classical thermodynamics, the compression and expansion of a piston containing an ideal gas provides one of the simplest scenarios for the theory. Starting from equilibrium, external work is required to compress the piston into a smaller volume while work is produced during the reverse process. In this case, the control parameter  $\lambda(t)$  is simply the piston's position as a function of time.

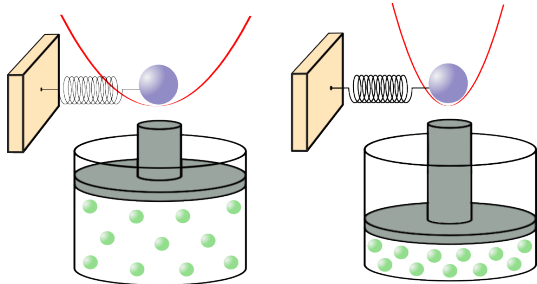


FIG. 4. A schematic representation of a piston showing two different volumes, analogous to a particle trapped in a harmonic potential with two corresponding trap stiffnesses.

This emblematic macroscopic scenario can be directly mapped to the mesoscopic regime using an optically trapped micro-sphere as a prototype model for a Brownian particle in a harmonic potential, as illustrated in Fig. 4. In this analogy, the piston role is played by a dynamically controlled optical potential  $U(x, t) = \frac{1}{2}\kappa(t)x^2$ , and the control parameter is the trap stiffness of the optical potential, i.e.,  $\lambda(t) \equiv \kappa(t)$ .

In the *compression process*, the trap stiffness increases, restricting the particle to a smaller region. This is analogous to the piston case. Conversely, as the stiffness decreases, the trap becomes weaker, allowing the particle to access a larger volume, representing the *expansion process*. Figure 5 shows this connection explicitly with potentials reconstructed directly from experiments at different trap strengths. To calculate the potential directly from the particle's position data, one starts by allowing it to be in thermal equilibrium with the environment (fluid) at temperature  $T$ . Thus, its probability distribution follows a Maxwell-Boltzmann distribution:

$$P(x) = P_0 \exp\left[-\frac{U(x)}{k_B T}\right], \quad (16)$$

where  $P_0$  is a normalization factor, such that  $\int P(x)dx = 1$ . Hence, the potential  $U(x)$  can be readily determined by

$$U(x) = -k_B T \log[P(x)] + U_0, \quad (17)$$

where  $U_0$  is an arbitrary additive constant.

This simple experiment provides a quick and essentially model-independent outline of the optical potential, which is very practical in the lab but usually does not have enough precision. In section III B, we present a more precise and robust calibration method for the case of a harmonic potential.

Since the particle remains immersed in a fluid with fixed temperature  $T$ , performing isothermal processes is straightforward. The control protocol  $\lambda(t)$  can easily be programmed

to different types of profiles, enabling different experiments. For simplicity, here we focus on a linear protocol:

$$\lambda(t) = \lambda_i + \frac{\Delta\lambda}{\tau_P}t, \quad (18)$$

where  $\Delta\lambda = \lambda_f - \lambda_i$  is the amplitude of modulation, and  $\tau_P$  is the time execution of the protocol.

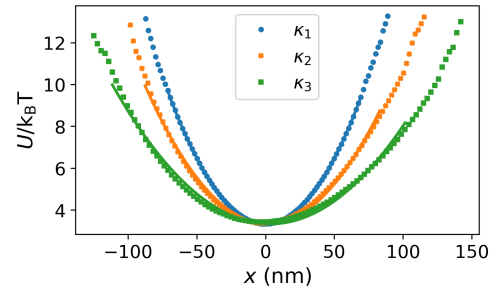


FIG. 5. Measured harmonic potentials for different force constants  $\kappa$  (control parameter), with  $\kappa_1 > \kappa_2 > \kappa_3$ . Results were obtained from position histograms of a trapped  $2 \mu\text{m}$  silica bead. The value of  $\kappa$  is proportional to the laser intensity, and in experiments, the compression and expansion protocols are executed via intensity modulation.

The particle's Hamiltonian is given by  $H(t) = p^2/2m + U(t)$ , where  $p$  is the particle momentum and  $U(t)$  is the trapping harmonic potential

$$U(t) = \frac{\lambda(t)x^2}{2}. \quad (19)$$

Thus, the partition function for a given  $\lambda$  is

$$Z = \int_{-\infty}^{+\infty} dx \int_{-\infty}^{+\infty} dp e^{-H/k_B T} = Z_p \sqrt{\frac{2\pi k_B T}{\lambda}}, \quad (20)$$

where  $Z_p = \int_{-\infty}^{+\infty} dp e^{-p^2/2mk_B T} = \sqrt{2\pi mk_B T}$ .

For a finite-time process, the work relative to a single run of the protocol can be computed using Eqs. (5), (18), and (19):

$$W = \frac{\Delta\lambda}{2\tau_P} \int_0^{\tau_P} x^2(t) dt. \quad (21)$$

For an ensemble of trajectories, the average work is

$$\langle W \rangle = \int_0^{\tau_P} dt \frac{d\lambda(t)}{dt} \left\langle \frac{\partial U(x, \lambda)}{\partial \lambda} \right\rangle = \frac{\Delta\lambda}{2\tau_P} \int_0^{\tau_P} \langle x^2(t) \rangle dt. \quad (22)$$

From Eq. (12) and the initial condition obtained from the equipartition theorem of energy, i.e.,  $\langle x^2(0) \rangle = k_B T / \lambda_i$ , it is possible to estimate  $\langle x^2 \rangle$  and compute the average work.

Finally, given the Helmholtz free energy  $F := -k_B T \ln Z$ , one can obtain the  $\Delta F$  relative to the equilibrium states characterized by  $\lambda_i$  and  $\lambda_f$ :

$$\Delta F = -k_B T \ln \frac{Z_f}{Z_i} = -k_B T \ln \sqrt{\frac{\lambda_i}{\lambda_f}}. \quad (23)$$

Note that, given Eq. (3) for the second law, one can quickly identify this quantity as the minimum amount of energy necessary to pay for driving the particle's state from  $\lambda_i$  to  $\lambda_f$ , such that  $\langle W \rangle \geq \Delta F$ , where the equality is only achieved by infinite-time protocols (quasi-statically).

In conclusion, it is possible to gather statistics that recover meaningful thermodynamic quantities by measuring the particle's position during many repetitions of the same protocol. This can be done both at the level of individual trajectories—by examining how work evolves during a single protocol run—and at the ensemble level by repeating the process  $N$  times. A critical experimental challenge, however, lies in accurately characterizing and controlling the external potential experienced by the particle.

### III. EXPERIMENT

This section presents the experimental part of this work, demonstrating how to verify the fluctuation theorems using a custom-built optical tweezers setup. First, we introduce the experimental configuration and outline the calibration process for characterizing the harmonic potential. Then, we present the results and their analysis.

In short, the physical system under investigation is a trapped  $2\ \mu\text{m}$  silica micro-sphere (bead) manipulated dynamically using optical fields. Controlling the optical potential while simultaneously recording the bead's position, we can calculate the stochastic trajectories introduced in section II B and use the gathered statistics of the ensemble to verify Eqs. (13) and (15).

#### A. Experimental setup

The experimental setup is illustrated in Figure 6. A 1064 nm infrared (IR) laser (FORTE 02163 1064-SLM, supply 93580 LD 3000, Laser Quantum) is used to trap the particles. The laser is connected to two perpendicular acousto-optic deflectors (AODs), specifically the Optoelectronic DT-SXY model, which allow precise control over the beam's intensity and angular position.

The 2-axis AOD utilizes piezoelectric transducers to modulate an optical media ( $\text{TeO}_2$  crystal). When a radiofrequency signal from a function generator (AFG3102) drives the piezoelectric device, an acoustic wave propagates through the crystal, diffracting the passing light. By aligning the system with the first diffraction order ( $m=1$ ), we gain control over the beam's intensity and angular position by adjusting the amplitude and frequency of the radiofrequency signal. The two perpendicular AODs enable independent control of the beam's position along the  $x$  and  $y$  axes, but here, we will mainly focus the discussion and analysis on one of these directions.

A  $63\times$  immersion objective lens ( $\text{NA} = 1.32$ , Leica Germany HCX PL APO) focuses the IR beam to trap the particle. A telescope composed of two lenses collimates and magnifies the trapping laser, ensuring it fully occupies the entrance pupil of the objective. This maximizes trapping efficiency, as the

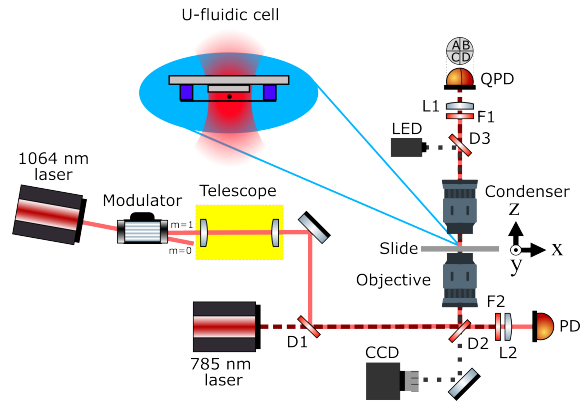


FIG. 6. The experimental setup consists of a trapping system with a 1064 nm infrared laser passing through to a 2-axis acousto-optic deflector (AOD). A telescope expands the beam waist to fill the entrance of a  $63\times$  immersion objective lens ( $\text{NA} = 1.32$ , Leica Germany HCX PL APO). For position detection, a 785 nm laser is aligned with the trapping laser. A condenser collects the scattered light and directs it through lens L1 to focus it onto a Quadrant Photodiode (QPD). Additionally, a white LED and a CCD camera (Mikrotron MC 1310) are also used to visualize and record the particle's position. Mirrors and dichroic filters (D1, D2, D3) guide the beams. A notch filter (F1) blocks all wavelengths except the 785 nm light, allowing it to reach the QPD, while a long-pass filter (F2) prevents the 785 nm light from reaching the photodetector (PD) used to monitor the trapping IR laser. Lens L2 focuses the infrared beam onto the PD to maximize its signal. The inset at the top depicts the custom-designed U-shaped fluidic cell that enables long-duration measurements by preventing interference from other particles.

gradient force, which is proportional to the intensity gradient, is optimized by tightly focusing the beam. After the objective, a sample holder connected to a 3D nanopositioning stage allows for precise adjustments of the sample's position. We trap low-concentration  $2\ \mu\text{m}$  silica beads within a U-fluidic cell (see inset in Fig. 6). This homemade cell is constructed by gluing a slide to a coverslip with double-sided tape and attaching a glass cylinder at the center to minimize the distance between surfaces to approximately  $50\ \mu\text{m}$ . This design can significantly reduce the influx of particles in the measurement region, facilitating long-term data acquisition [69]. For measurements, the monitored particle is captured at the edges of this region and optically dragged into the central area.

For particle visualization, we use a bright-field CCD camera (Mikrotron MC 1310) and a white LED for illumination. The trapped particles are tracked using a Quadrant Photodiode Detector (QPD) to achieve the high sampling rate necessary for out-of-equilibrium processes. A **low-power 785 nm laser** (Thorlabs LP785-SF20) is integrated into the trapping path and aligned collinearly with the trapping laser. The interference between the trapping and scattered fields produces a position-dependent pattern, collected by a condenser with numerical aperture  $\text{NA} = 0.53$  (Leica 521500) and directed to a homemade QPD. The QPD output voltage signals ( $A$ ,  $B$ ,  $C$ , and  $D$ ), from which the particle's center of mass positions are

calculated as:

$$x_{\text{QPD}} = (A + C) - (B + D), \quad (24)$$

$$y_{\text{QPD}} = (A + B) - (C + D). \quad (25)$$

Finally, the control of the function generator, along with readings from the QPD voltages and the photodetector (PD) PDA36A-EC—which monitors the infrared beam’s power—is managed using a high-speed multi-function data acquisition (DAQ) board (PXI 4472).

## B. Characterizing harmonic potentials

Various methods exist to determine the trap stiffness,  $\kappa_{x(y)}$ , and the factor  $S_{x(y)}$ , which relates the QPD output to actual position readings. Section IID 2, in Eq.(17), discussed one of the simplest. However, the power spectral density (PSD) analysis [71] is the most reliable approach [40], and it is the method used here. The procedure involves trapping a particle in a static potential and recording the position  $x(t)$  at a sampling frequency  $f_s$  over a time interval  $T_s$ . The analysis focuses on the  $x$ -axis, but the same applies to the  $y$  and  $z$ -axes.

From the position data  $x(t)$ , a numerical discrete Fourier transform can convert it to the frequency domain, yielding  $\tilde{x}(f)$ . The PSD is then calculated as:

$$P(f) = \lim_{T_s \rightarrow +\infty} \frac{|\tilde{x}(f)|^2}{T_s}. \quad (26)$$

For PSD computation, we employed Welch’s method [72], using an acquisition rate at  $f_s = 100$  kHz and  $T_s = 30$  s. This resulted in the number of points  $N_{\text{FFT}} = 8 \times 10^5$  used for  $\kappa_x$  and  $S_x$  characterization, with a 90% overlap between segments. Figure 7 displays the PSD from experimental data of a  $2 \mu\text{m}$  silica bead trapped at three different laser powers. Higher laser power corresponds to increased trap stiffness and reduced mean squared displacement within the trap. At each power level, 10 measurements were taken, and the presented PSD represents the average of these measurements. Laser power is directly controlled via the AOD amplitude channel.

The analytical PSD for a harmonic trap can be expressed by [40, 71]:

$$P(f) = \frac{S_x^2 D}{2\pi^2(f^2 + f_c^2)}, \quad (27)$$

where  $D = k_B T / \gamma$  is the diffusion coefficient,  $S_x$  is the amplification factor converting QPD voltage output to position ( $x(t) = x_{\text{QPD}}(t) / S_x$ ),  $f_c = \kappa_x / 2\pi\gamma$  is the corner frequency, and  $\gamma = 6\pi\eta R$  is the particle’s friction coefficient ( $\eta$  is the medium viscosity and  $R$  is the particle radius). Detailed derivations are in Ref. [69]. From data and using the least squares fit [73], one can extract the trap stiffness  $\kappa_x$  and the amplification factor  $S_x$ .

Figure 8 presents the calibration curves for trap stiffness and amplification factor obtained from the PSD data. A linear relationship between trap stiffness and laser power is observed as anticipated. Notice that the amplification factor also varies slightly with laser power due to radiation pressure changing

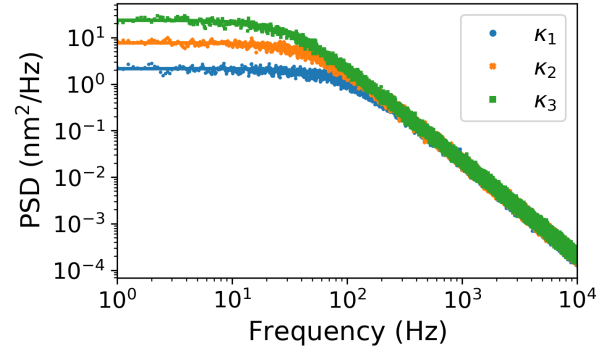


FIG. 7. Power spectra density (PSD) analysis of a  $2 \mu\text{m}$  silica bead trapped at three different laser powers, increasing from green to blue ( $\kappa_1 > \kappa_2 > \kappa_3$ ). Higher laser power increases trap stiffness and lowers the PSD baseline plateau at low frequencies.

the equilibrium position along the  $z$ -axis, which affects  $S_{x(y)}$ . We establish a calibration curve for the QPD response:

$$S_{\text{fit},x} = a_S V_{\text{PD}} + b_S, \quad (28)$$

where  $V_{\text{PD}}$  is the infrared PD signal, and  $a_S$  and  $b_S$  are the slope and intercept from the linear fit (inset of Fig. 8).

By simultaneously recording the QPD ( $x_{\text{QPD}}$ ) and infrared PD signals, we determine the particle’s center of mass position:

$$x(t) = \frac{x_{\text{QPD}}(t)}{S_{\text{fit},x}}, \quad (29)$$

and estimate the trap stiffness:

$$\kappa = a_{\text{TS}} V_{\text{PD}} + b_{\text{TS}}, \quad (30)$$

where  $a_{\text{TS}}$  and  $b_{\text{TS}}$  are the slope and intercept from the linear fit, as shown in Fig. 8.

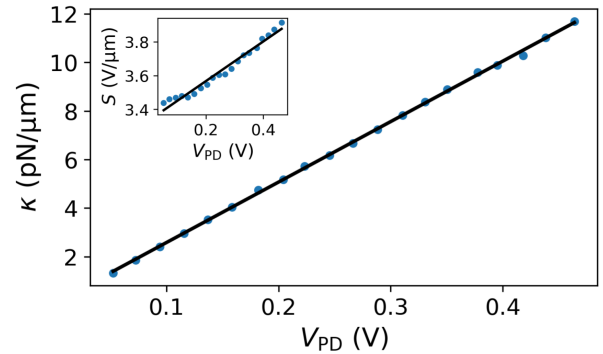


FIG. 8. Calibration curves for trap stiffness and amplification factor obtained from PSD fits as a function of the infrared laser power, monitored by  $V_{\text{PD}}$ . The trap stiffness calibration yields a slope  $a_{\text{TS}} = 24.9 \pm 0.1$  (pN/ $\mu\text{m}$ )/V and intercept  $b_{\text{TS}} = 0.09 \pm 0.04$  pN/ $\mu\text{m}$ . The amplification factor calibration (inset) provides  $a_S = 1.17 \pm 0.05 \mu\text{m}^{-1}$ , and  $b_S = 3.33 \pm 0.01$  V/ $\mu\text{m}$ .

## C. Results and analysis

### 1. Protocol application & work inference

After characterizing the optical potential, the protocols for *compression* and *expansion* (see Section IID 2) were applied to the same particles used in the calibrations, using the linear protocol in Eq. (18). To ensure thermal equilibrium, the laser power is held constant at the initial state  $\lambda_i$  for a time interval  $\tau_{eq} > \tau_R$ , where  $\tau_R = \gamma/\lambda_i$  is the relaxation time in the state  $\lambda_i$ . Fig. 9 shows the measured position variance of the particle,  $\sigma_x^2$ , during the equilibration period at  $\lambda_i = 1.5$  pN/ $\mu\text{m}$ , demonstrating that  $\tau_{eq} = 20$  ms is sufficient for the variance to stabilize and reach a steady state even for the weakest trap.

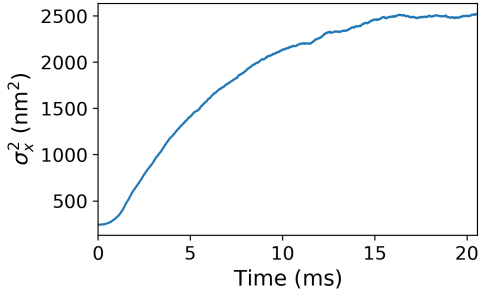


FIG. 9. Position variance during thermalization at  $\lambda_i = 1.5$  pN/ $\mu\text{m}$ , starting from  $11\lambda_i$ . A linear protocol with  $\tau_P = 0.1\tau_R$  is applied, followed by thermalization with equilibration time  $\tau_{eq} = 20$  ms. This case was selected because it is the largest step executed in the experiment, with the longest equilibration time.

Post-equilibration, the protocol is executed by linearly increasing the trap stiffness until it reaches a final value  $\lambda_f > \lambda_i$ , and the laser intensity is maintained until the particle thermalizes again at  $\lambda_f$ . This constitutes the *compression* process. To execute the *expansion* protocol, after the equilibration period at  $\lambda_f$ , the particle is linearly returned to the initial value  $\lambda_i$ , and the process is repeated thousands of times.

To calculate the work during the protocol execution, one can discretize Eq. (21), considering that data is acquired at regular time intervals  $\Delta t = 1/f_s$  [74], leading to the cumulative work at instant  $t_n$  given by

$$W_n = \frac{1}{2}\Delta t \sum_{j=0}^{n-1} \frac{\lambda_{j+1} - \lambda_j}{\Delta t} x_j^2 = \frac{1}{2} \sum_{j=0}^{n-1} (\lambda_{j+1} - \lambda_j) x_j^2, \quad (31)$$

where  $t_j = j\Delta t$  with  $j = 0, 1, 2, \dots, n$ . For a protocol with duration  $\tau_P$ , the temporal evolution of the work can be expressed in terms of the time step  $n$ . Therefore, the final work value is calculated using  $n = \tau_P/\Delta t$ . It is important to note that work only contributes when  $d\lambda/dt \neq 0$ ; which means that the thermalization period does not contribute to work.

After applying the protocol and recording the position of the particle,  $x_j$ , simultaneously with the stiffness of the trap,  $\lambda_j$ , one has all the information needed to compute the relevant thermodynamic quantities. To illustrate the experimental results of this step, Figure 10 shows the stochastic position

measurements for 500 repetitions of the compression protocol, with  $\tau_P = 0.1\tau_R$  and  $\Delta\lambda = 10\lambda_i$ .

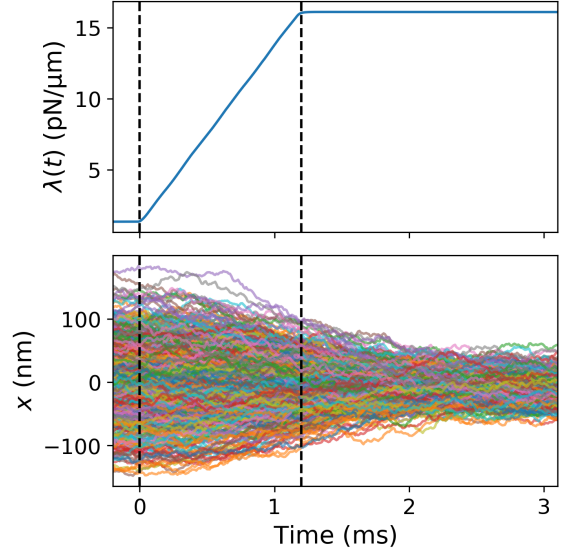


FIG. 10. Measured control parameter (top) and 500 stochastic trajectories (bottom) for linear compression protocol with  $\tau_{eq} = 20$  ms,  $\lambda_i = 1.5$  pN/ $\mu\text{m}$ ,  $\Delta\lambda = 10\lambda_i$ , and  $\tau_P = 0.1\tau_R$ , where  $\tau_R = \gamma/\lambda_i \approx 12$  ms is the relaxation time in the state  $\lambda_i$ . The black dashed lines indicate the beginning and end of the protocol.

Using Eq. (31) and the acquired data, one calculates the fluctuating work across the stochastic trajectories. Figure 11 displays the results for 10 distinct runs of the same protocol.

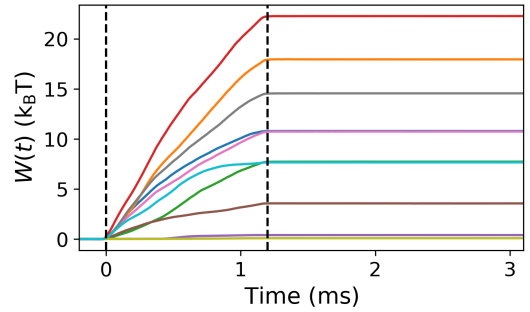


FIG. 11. Temporal evolution of work for 10 arbitrary trajectories using the same linear compression protocol, with  $\lambda_i = 1.5$  pN/ $\mu\text{m}$ ,  $\Delta\lambda = 10\lambda_i$ , and  $\tau_P = 0.1\tau_R$ , where  $\tau_R \approx 12$  ms, and  $\tau_{eq} = 20$  ms. The black dashed lines indicate the beginning and end of the protocol.

After a large number of repetitions ( $N = 10^4$ ) of the same protocol, a histogram is produced using the calculated work, and the probability density function (pdf),  $P(W)$ , is determined, ensuring  $\int P(W) dW = 1$ . Figure 12 shows the results for two modulation amplitudes ( $\Delta\lambda$ ) and three different protocol durations ( $\tau_P$ ). For each colored solid curve, a vertical dashed line indicates the average work, while the free energy change,  $\Delta F$ , is marked by the black vertical dashed lines. As expected, the measured work exhibits significant fluctuations with  $\langle W \rangle > \Delta F$ . Fig. 12 also allow a direct comparison of the

work pdf between far-from-equilibrium (quick,  $\tau_P = 0.1\tau_R$ ) and near-equilibrium (slower,  $\tau_P = 2\tau_R$ ) protocols.

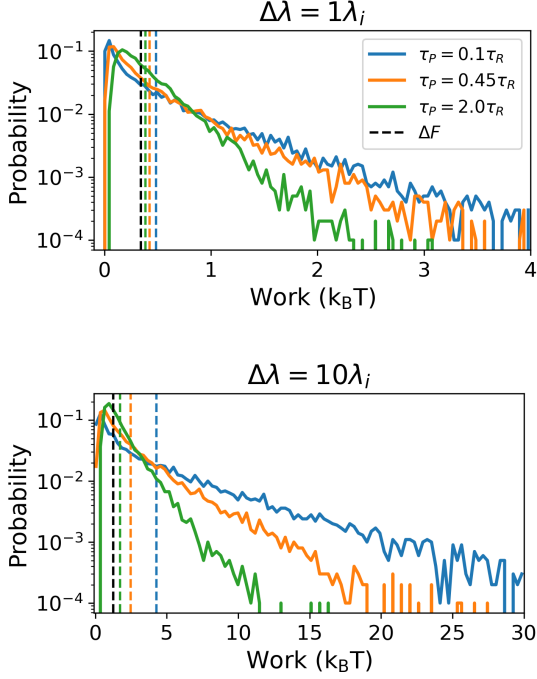


FIG. 12. Work probability distributions (colored solid lines) and the respective average value of work (same color dashed lines) for protocol times:  $\tau_P = \{0.1\tau_R, 0.45\tau_R, 2\tau_R\}$ , in blue, orange, and green respectively. Two modulation amplitudes were considered,  $\Delta\lambda = \lambda_i$  (top) and  $\Delta\lambda = 10\lambda_i$  (bottom). Results are from  $N = 10^4$  trajectories of forward linear protocols with  $\tau_{eq} = 20$  ms,  $\lambda_i = 1.5$  pN/ $\mu$ m, and  $\tau_R \approx 12$  ms. The black dashed line indicates the free energy difference. The number of bins used for the histograms is 100.

Examining these distributions, we see that the work variance decreases, and the average work approaches the free energy difference as the protocol is driven more slowly. This behavior is consistent with the second law, as described by Eq. (3). In the ideal quasistatic scenario (where the process is infinitely slow), one would expect a succession of equilibrium states with a narrow distribution centered at the free energy difference  $\Delta F$ , the minimal required to change the state.

Notably, although the average work never falls below the free energy difference, individual trajectories can occasionally be below  $\Delta F$ . These instances have sometimes been called “violations” of the second law. The frequency of these rare events increases as the process deviates further from equilibrium, i.e., with larger modulation amplitudes and shorter protocol durations. Nevertheless, the work distributions always satisfy  $\int_{-\infty}^{\Delta F} P(W) dW < \int_{\Delta F}^{\infty} P(W) dW$ .

## 2. Jarzynski equality

Building on previous steps, we can verify Jarzynski’s equality, Eq. (13). As mentioned earlier, the exact free energy dif-

ference for the linear protocol is given by Eq. (23). Therefore, the right-hand side of Eq. (13) can be expressed simply as

$$e^{-\Delta F/k_B T} = \frac{Z_f}{Z_i} = \sqrt{\frac{\lambda_i}{\lambda_f}}, \quad (32)$$

where  $Z_{\{i,f\}}$  and  $\lambda_{\{i,f\}}$  are the partition functions and the trapping control parameters of the initial and final states.

Using the work statistics obtained from the experimental data, the left-hand side of Eq. (13) can also be calculated.

The uncertainty of  $e^{-\Delta F/k_B T}$  is calculated using uncertainty propagation:

$$\delta[e^{-\Delta F/k_B T}] = \frac{1}{2} \sqrt{\left(\frac{\delta\lambda_i}{\lambda_f}\right)^2 + \left(\frac{\lambda_i\delta\lambda_f}{\lambda_f^2}\right)^2}, \quad (33)$$

where  $\delta\lambda(t) = \sqrt{(\delta m_{TS} V_{PD}(t))^2 + (\delta V_{PD}(t) m_{TS})^2 + (\delta b_{TS})^2}$  represents the uncertainties in the trap stiffness at the initial ( $\delta\lambda_i$ ) and final ( $\delta\lambda_f$ ) states. The uncertainty of  $\delta[\exp(-W/k_B T)]$  is determined by dividing the dataset into subgroups. Specifically, we compute  $\{\exp(-W/k_B T)\}_{i=1,\dots,1000}$  for 10 groups, each containing 1000 trajectories. The uncertainty  $\delta[\exp(-W/k_B T)]$  is then obtained from the standard deviation of these values, calculated as  $\sigma_{\{\exp(-W/k_B T)\}_{i=1,\dots,1000}} / \sqrt{10}$ .

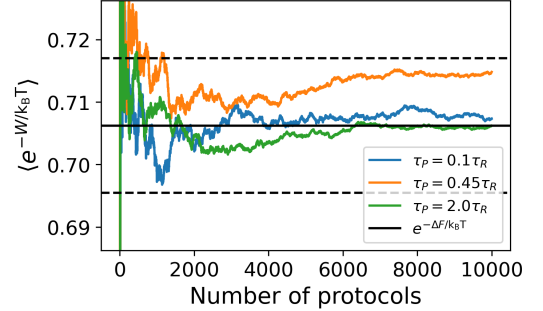


FIG. 13. Convergence of  $\langle e^{-W/k_B T} \rangle$  versus the number of experimental executions of the linear compression protocol for  $\Delta\lambda = \lambda_i$  and same parameters of Fig. 12. The black solid center line corresponds to  $e^{-\Delta F/k_B T}$ , and dashed lines represent the uncertainty range.

Figure 13 illustrates the behavior of  $\langle e^{-W/k_B T} \rangle$  as a function of the number of protocol repetitions. Note that the average value converges towards a stable value as the number of trajectories increases. Ideally, an infinite number of samples would be required for an exact verification, but results show that  $N \approx 2000$  realizations are sufficient to confirm the Jarzynski equality within the calculated uncertainties.

Figure 14 presents the verification of the Jarzynski equality across different protocol durations (from  $\tau_P = 0.1\tau_R$  to  $\tau_P = 2\tau_R$ ) and modulation amplitudes ( $\Delta\lambda = \{\lambda_i, 3\lambda_i, 10\lambda_i\}$ ), all with  $N = 10^4$  realizations. The results indicate that for small amplitude modulation ( $\Delta\lambda = \lambda_i$ ), the Jarzynski equality holds consistently across all examined protocol durations. More specifically, the value of  $e^{-\Delta F/k_B T}$  obtained from the PD readings during the initial and final equilibrium periods aligns

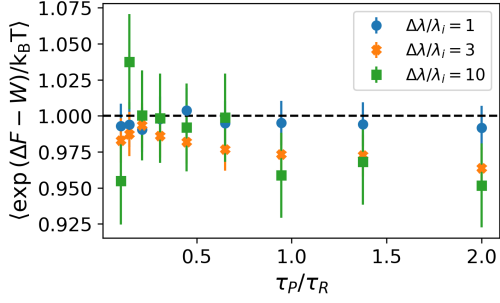


FIG. 14. Verification of Jarzynski equality for a linear compression. The average  $\langle e^{(\Delta F - W)/k_B T} \rangle$  for different durations  $\tau_P$  and modulation amplitudes:  $\Delta\lambda/\lambda_i = \{1, 3, 10\}$ , in blue, orange, and green, respectively. Each point represents data from  $10^4$  realizations of the experiment at the same conditions. The black dashed line shows the (exact) expected value, and the bars indicate the uncertainty for each point.

well with  $\langle e^{-W/k_B T} \rangle$  obtained from the work distributions. For larger values of  $\Delta\lambda$ , better agreement is observed with shorter protocol times. This discrepancy may be due to the amplification factor  $S_x$  depending on the power of the trapping beam.

Interestingly, in the linear expansion protocol, the trap stiffness decreases over time, i.e.,  $d\lambda/dt < 0$ , leading to negative work values since  $\langle x^2 \rangle > 0$ , as shown in Fig. 15. It is important to understand that here the rare events (occurring at the tails of the probability distributions) significantly impact the calculation of  $\langle e^{-W/k_B T} \rangle$ . This makes it much harder to verify Jarzynski's equality with a limited number of protocol repetitions ( $N$ ) since a very large  $N$  is often necessary. Rare events significantly affect how quickly results converge, as illustrated in Fig. 16. Most repetitions do not have much influence on the average value, while a few rare events greatly affect the exponential average [75]. In this case, it's better to use Crooks' relation, Eq. (15), because it uses the ratio of probabilities and is less affected by these rare events.

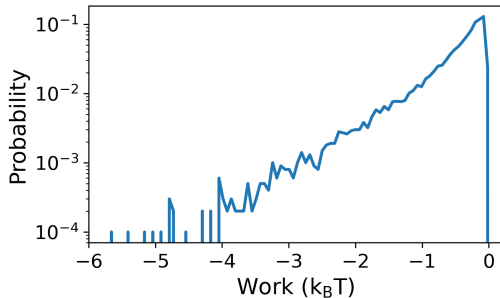


FIG. 15. Probability distributions of work for the linear expansion protocol with  $N = 10^4$  trajectories,  $\tau_{eq} = 20$  ms,  $\lambda_i = 1.5$  pN/ $\mu$ m,  $\tau_P = 0.1\tau_R$ ,  $\tau_R \approx 12$  ms,  $\Delta\lambda = 10\lambda_i$ , and using 100 bins.

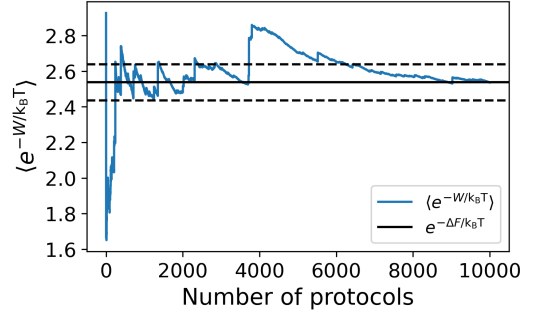


FIG. 16. Convergence of  $\langle e^{-W/k_B T} \rangle$  versus the number of experimental executions of the linear expansion protocol for  $\Delta\lambda = 10\lambda_i$ ,  $\tau_P = 0.21\tau_R$ ,  $\tau_{eq} = 20$  ms,  $\lambda_i = 1.5$  pN/ $\mu$ m, and  $\tau_R \approx 12$  ms. The black dashed lines represent the uncertainty range. Notice the significant effect of rare events (sudden jumps) in the convergence.

### 3. Crooks fluctuation theorem

As introduced in Section II C, Crooks proposed Eq. (15), which relates the probabilities of work in a forward-protocol ( $P_F(W)$ ) and its backward (time-reversed) protocol ( $P_R(-W)$ ). In this experiment, the reverse (expansion) protocol was applied immediately after the forward (compression) protocol, as explained previously, always allowing for the required equilibration time before proceeding.

Figure 17 displays the stochastic work distributions from  $N = 10^4$  experimental realizations for two modulation amplitudes. As anticipated, the crossing point  $P_F(W) = P_R(-W)$  occurs precisely at the work value equal to the free energy difference  $\Delta F$ , as indicated by the vertical black dashed lines. This observation provides a straightforward method for estimating  $\Delta F$ . Moreover, it is worth noting that for this particular case, verifying this result from Crooks' theorem is easier and more robust than Jarzynski's because the intersection point is positioned near the peaks of the histograms, which minimizes the effect of rare events on the results.

Taking the *logarithm* of Eq. (15) yields

$$\ln \left[ \frac{P_F(W)}{P_R(-W)} \right] = \frac{W - \Delta F}{k_B T}, \quad (34)$$

allowing us to assess the validity of the relation for various work values, not just at the point where  $W = \Delta F$ . Figure 18 shows the experimental values of  $\ln \left[ \frac{P_F(W)}{P_R(-W)} \right]$  for different protocol durations and amplitudes. The data aligns with the linear function  $W - \Delta F = 0$  at lower work values with higher counts, while it scatters at larger work values due to rare events (lower counts). There is better agreement between experimental data and theoretical predictions for protocols with smaller modulation amplitudes and shorter durations, likely due to amplification factor miscalibration, like before. Nonetheless, the data remains consistent with the expected behavior and complies with the Crooks fluctuation theorem [75].

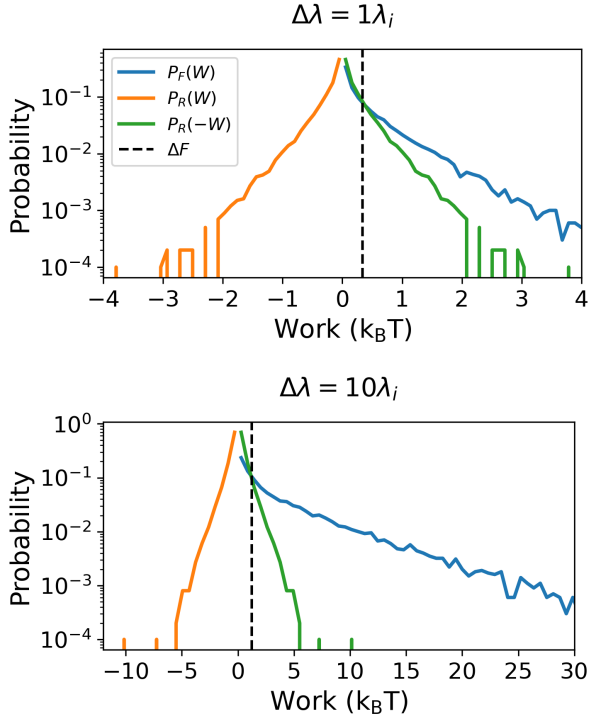


FIG. 17. Probability distributions  $P_F(W)$ ,  $P_R(W)$ , and  $P_R(-W)$  for  $10^4$  trajectories with  $\tau_{eq} = 20$  ms,  $\lambda_i = 1.5$  pN/ $\mu$ m,  $\tau_p = 0.1\tau_R$ , with  $\tau_R = \gamma/\lambda_i \approx 12$  ms, and  $\Delta\lambda = \lambda_i$  (top) and  $\Delta\lambda = 10\lambda_i$  (bottom). The black dashed line indicates the free energy difference  $\Delta F$ .

#### IV. DISCUSSION AND CONCLUSIONS

This work helps spread the knowledge of stochastic thermodynamics by introducing and measuring the Jarzynski and Crooks relations, together with key ideas by Sekimoto. Here, we present a home-built apparatus and explain thoroughly the methods for measuring and validating these outstanding results through experiments with optical tweezers. These non-equilibrium work relations connect an equilibrium quantity—the free energy difference—and out-of-equilibrium measurements. Notably, these relations enable the determination of free energy differences without performing a quasistatic process, which would require prohibitively long times.

The experiment used finite time *compression* and *expansion* protocols on an optically trapped Brownian particle. By modulating the intensity of the trapping beam, we can dynamically adjust the parameters of the external potential, thereby altering the state of the particle. By characterizing the optical potential at various laser intensities and analyzing the particle’s trajectory, we can compute the fluctuating work applied during each protocol execution to construct probability distributions from an ensemble of repetitions. The calculated free energy values for the initial and final states, which are determined experimentally through the well-characterized optical potential, can be directly compared with those obtained experimentally from the work probability distributions.

Regarding the Jarzynski equality, the experimental values

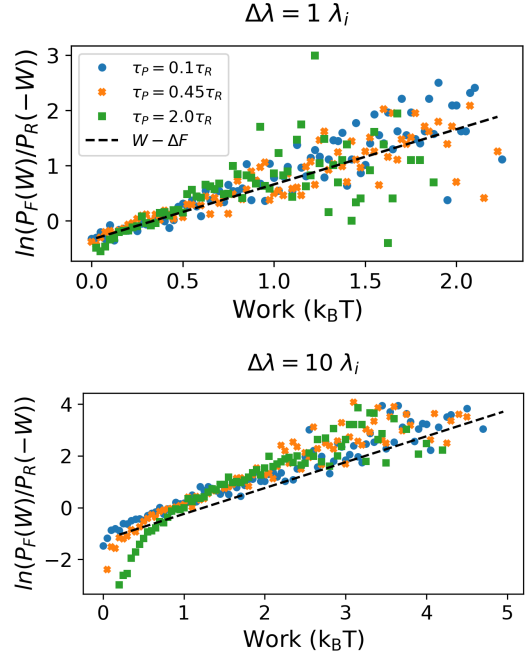


FIG. 18. Verification of Crooks Fluctuation Theorem for  $\Delta\lambda = \lambda_i$  (top) and  $\Delta\lambda = 10\lambda_i$  (bottom). Experimental values of  $\ln \left[ \frac{P_F(W)}{P_R(-W)} \right]$  for 10,000 trajectories with  $\lambda_i = 1.5$  pN/ $\mu$ m and different  $\tau_p$ .

of  $\langle e^{-W/k_B T} \rangle$  were verified to be consistent with  $e^{-\Delta F/k_B T}$  after a few thousand realizations of the compression protocol, being largely stable across all parameter sets. We experimented with different modulation amplitudes and protocol times to confirm the robustness of this convergence. For the expansion protocol, due to the negative work values, we showed that the Jarzynski average can be significantly affected by rare events.

Applying the Crooks relation, we showed that it is more robust and less sensitive to rare events, and we also obtained a good agreement between theory and experiments. This agreement is stronger for higher counts, with some scattering observed in the regions corresponding to rare events.

Overall, both fluctuation theorems were verified experimentally, largely matching theoretical predictions despite the better agreement for lower modulation amplitudes and shorter protocol time. The difference at higher intensities results from a systematic miscalibration of the amplification factor, sensitive to the radiation pressure [76]. However, this systematic error introduces only minor variations which do not deviate significantly from what is expected. These results show the versatility of optical tweezers for experiments to test and explore fundamental principles in stochastic thermodynamics.

The successful hands-on verification of fundamental fluctuation theorems, such as the Jarzynski Equality and Crooks’ Relation, highlights the relative simplicity of this approach to explore and deepen the understanding of non-equilibrium thermodynamics experimentally, hopefully helping to inspire new generations of scientists to advance the field further.

## V. ACKNOWLEDGMENTS

TTM acknowledges the support from Fundação Coordenação de Aperfeiçoamento de Pessoal de Nível Superior for PROEX (Programa de Excelência Acadêmica, 88887.370240/2019-00) and CAPES-PRINT (PRINT - Programa Institucional de Internacionalização, 88887.716077/2022-00). SRM acknowledges support from FAPESP (Fundação de Amparo à Pesquisa do Estado de São

Paulo), Grants no. 2019/27471-0, 2013/07276-1. A.H.A.M. acknowledges support from the National Science Centre, Poland Grant OPUS-21 (No. 2021/41/B/ST2/03207). The authors thank Leonardo Paulo Maia and Paulo Henrique Souto Ribeiro for inspiring discussions and Diogo de Oliveira Soares Pinto, Frederico Borges de Brito, and René Alfonso Nome Silva for stimulating and encouraging this line of research in São Carlos since the beginning.

- 
- [1] M. W. Zemansky, *Heat and thermodynamics*, 3rd ed. (McGraw-Hill, New York, 1951).
- [2] H. B. Callen, *Thermodynamics and an introduction to thermostatistics*, 2nd ed. (Wiley, New York, 1985).
- [3] D. Kondepudi and I. Prigogine, *Modern thermodynamics*, 2nd ed. (John Wiley, New York, 2015).
- [4] X. Fang, K. Kruse, T. Lu, and J. Wang, Nonequilibrium physics in biology, *Rev. Mod. Phys.* **91**, 045004 (2019).
- [5] J. D. Bekenstein, Black holes and the second law, *Lettere al Nuovo Cimento* (1971-1985) **4**, 737 (1972).
- [6] J. D. Bekenstein, Black holes and entropy, *Phys. Rev. D* **7**, 2333 (1973).
- [7] G. W. Gibbons and S. W. Hawking, Cosmological event horizons, thermodynamics, and particle creation, *Phys. Rev. D* **15**, 2738 (1977).
- [8] F. Reif, *Fundamentals of statistical and thermal physics*, international ed. (McGraw-Hill, Tokyo, 1985).
- [9] A. Einstein, On the motion of small particles suspended in liquids at rest required by the molecular-kinetic theory of heat, *Annalen der Physik* **17**, 208 (1905).
- [10] J. Perrin, Mouvement brownien et grandeurs moléculaires, *Radium (Paris)* **6**, 353 (1909).
- [11] F. Ritort, Nonequilibrium fluctuations in small systems: From physics to biology, *Advances in chemical physics* **137**, 31 (2008).
- [12] U. Seifert, Stochastic thermodynamics, fluctuation theorems and molecular machines, *Reports on progress in physics* **75**, 126001 (2012).
- [13] H. G. Schuster, *Nonequilibrium statistical physics of small systems* (John Wiley, New York, 2013).
- [14] D. J. Evans, E. G. D. Cohen, and G. P. Morriss, Probability of second law violations in shearing steady states, *Phys. Rev. Lett.* **71**, 2401 (1993).
- [15] D. J. Evans and D. J. Searles, The fluctuation theorem, *Adv. Phys.* **51**, 1529 (2002).
- [16] G. Gallavotti and E. G. D. Cohen, Dynamical ensembles in nonequilibrium statistical mechanics, *Phys. Rev. Lett.* **74**, 2694 (1995).
- [17] J. L. Lebowitz and H. Spohn, A gallavotti-cohen-type symmetry in the large deviation functional for stochastic dynamics, *J. Stat. Phys.* **95**, 333 (1999).
- [18] J. Kurchan, Fluctuation theorem for stochastic dynamics, *J. Phys. A* **31**, 3719 (1998).
- [19] D. J. Searles, L. Rondoni, and D. J. Evans, The steady state fluctuation relation for the dissipation function, *J. Stat. Phys.* **128**, 1337 (2007).
- [20] D. J. Evans, D. J. Searles, and S. R. Williams, On the fluctuation theorem for the dissipation function and its connection with response theory, *J. Chem. Phys.* **128**, 014504 (2008).
- [21] U. Seifert, Entropy production along a stochastic trajectory and an integral fluctuation theorem, *Phys. Rev. Lett.* **95**, 040602 (2005).
- [22] L. Puglisi, A. Rondoni, and A. Vulpiani, Relevance of initial and final conditions for the fluctuation relation in markov processes, *J. Stat. Mech.* , P08010 (2006).
- [23] C. Jarzynski, Nonequilibrium equality for free energy differences, *Physical Review Letters* **78**, 2690 (1997).
- [24] G. E. Crooks, Nonequilibrium measurements of free energy differences for microscopically reversible markovian systems, *Journal of Statistical Physics* **90**, 1481 (1998).
- [25] J. Liphardt, S. Dumont, S. B. Smith, I. Tinoco, and C. Bustamante, Equilibrium information from nonequilibrium measurements in an experimental test of jarzynski's equality, *Science* **296**, 1832 (2002).
- [26] D. Collin, F. Ritort, C. Jarzynski, S. B. Smith, I. Tinoco Jr, and C. Bustamante, Verification of the crooks fluctuation theorem and recovery of rna folding free energies, *Nature* **437**, 231 (2005).
- [27] N. Garnier and S. Ciliberto, Nonequilibrium fluctuations in a resistor, *Physical Review E* **71**, 060101 (2005).
- [28] F. Douarche, S. Ciliberto, and A. Petrosyan, Estimate of the free energy difference in mechanical systems from work fluctuations: experiments and models, *Journal of Statistical Mechanics: Theory and Experiment* **2005**, P09011 (2005).
- [29] J. Koski, T. Sagawa, O. Saira, Y. Yoon, A. Kutvonen, P. Solinas, M. Möttönen, T. Ala-Nissila, and J. Pekola, Distribution of entropy production in a single-electron box, *Nature Physics* **9**, 644 (2013).
- [30] S. Ciliberto, Experiments in stochastic thermodynamics: Short history and perspectives, *Physical Review X* **7**, 021051 (2017).
- [31] J. Kurchan, A quantum fluctuation theorem (2001), arXiv:cond-mat/0007360 [cond-mat.stat-mech].
- [32] H. Tasaki, Jarzynski relations for quantum systems and some applications (2000), arXiv:cond-mat/0009244 [cond-mat.stat-mech].
- [33] C. Jarzynski and D. K. Wójcik, Classical and quantum fluctuation theorems for heat exchange, *Phys. Rev. Lett.* **92**, 230602 (2004).
- [34] M. Campisi, P. Talkner, and P. Hänggi, Fluctuation theorem for arbitrary open quantum systems, *Phys. Rev. Lett.* **102**, 210401 (2009).
- [35] M. Campisi, P. Hänggi, and P. Talkner, Colloquium: Quantum fluctuation relations: Foundations and applications, *Rev. Mod. Phys.* **83**, 771 (2011).
- [36] K. Funo, M. Ueda, and T. Sagawa, Quantum fluctuation theorems, *Thermodynamics in the Quantum Regime: Fundamental Aspects and New Directions* , 249 (2018).

- [37] J. Gemmer, M. Michel, and G. Mahler, *Quantum thermodynamics: Emergence of thermodynamic behavior within composite quantum systems*, Vol. 784 (Springer, 2009).
- [38] F. Binder, L. A. Correa, C. Gogolin, J. Anders, and G. Adesso, Thermodynamics in the quantum regime, *Fundamental Theories of Physics* **195**, 1 (2018).
- [39] N. M. Myers, O. Abah, and S. Deffner, Quantum thermodynamic devices: From theoretical proposals to experimental reality, *AVS quantum science* **4** (2022).
- [40] P. H. Jones, O. M. Maragò, and G. Volpe, *Optical tweezers: Principles and applications* (Cambridge University Press, 2015).
- [41] A. Ashkin, J. M. Dziedzic, J. Bjorkholm, and S. Chu, Observation of a single-beam gradient force optical trap for dielectric particles, *Optics Letters* **11**, 288 (1986).
- [42] J.-D. Wen, M. Manosas, P. T. Li, S. B. Smith, C. Bustamante, F. Ritort, and I. Tinoco, Force unfolding kinetics of rna using optical tweezers. i. effects of experimental variables on measured results, *Biophysical journal* **92**, 2996 (2007).
- [43] M. Manosas, J.-D. Wen, P. T. Li, S. B. Smith, C. Bustamante, I. Tinoco, and F. Ritort, Force unfolding kinetics of rna using optical tweezers. ii. modeling experiments, *Biophysical journal* **92**, 3010 (2007).
- [44] A. Alemany, A. Mossa, I. Junier, and F. Ritort, Experimental free-energy measurements of kinetic molecular states using fluctuation theorems, *Nature Physics* **8**, 688 (2012).
- [45] I. A. Martinez, E. Roldán, J. M. Parrondo, and D. Petrov, Effective heating to several thousand kelvins of an optically trapped sphere in a liquid, *Physical Review E* **87**, 032159 (2013).
- [46] P. A. Quinto-Su, A microscopic steam engine implemented in an optical tweezer, *Nature communications* **5**, 5889 (2014).
- [47] T. T. Martins and S. R. Muniz, Dynamically controlled double-well optical potential for colloidal particles (: SBFO-TON INTERNATIONAL OPTICS AN PHOTONICS CONFERENCE, 2021, São Carlos, SBFoton, 2021) pp. 1–4, DOI:10.1109/SBFotonIOPC50774.2021.9461866.
- [48] S. Krishnamurthy, R. Ganapathy, and A. Sood, Overcoming power-efficiency tradeoff in a micro heat engine by engineered system-bath interactions, *Nature Communications* **14**, 6842 (2023).
- [49] G. Nalupurackal, M. Lokesh, S. Suresh, S. Roy, S. Chakraborty, J. Goswami, A. Pal, and B. Roy, Towards stirling engine using an optically confined particle subjected to asymmetric temperature profile, *New Journal of Physics* (2023).
- [50] J. Gieseler, J. R. Gomez-Solano, A. Magazzù, I. P. Castillo, L. P. García, M. Gironella-Torrent, X. Viader-Godoy, F. Ritort, G. Pesce, A. V. Arzola, *et al.*, Optical tweezers—from calibration to applications: a tutorial, *Advances in Optics and Photonics* **13**, 74 (2021).
- [51] U. Seifert, Stochastic thermodynamics: principles and perspectives, *The European Physical Journal B* **64**, 423 (2008).
- [52] B. G. de Groot, A simple model for brownian motion leading to the langevin equation, *American journal of physics* **67**, 1248 (1999).
- [53] L. E. Reichl, *A modern course in statistical physics* (1999).
- [54] G. Volpe and G. Volpe, Simulation of a brownian particle in an optical trap, *American Journal of Physics* **81**, 224 (2013).
- [55] K. Sekimoto, Langevin equation and thermodynamics, *Progress of Theoretical Physics Supplement* **130**, 17 (1998).
- [56] A. Siegman, Simplified derivation of the fokker-planck equation, *American Journal of Physics* **47**, 545 (1979).
- [57] R. J. Harris and G. M. Schütz, Fluctuation theorems for stochastic dynamics, *Journal of Statistical Mechanics: Theory and Experiment* **2007**, P07020 (2007).
- [58] M. Esposito, U. Harbola, and S. Mukamel, Nonequilibrium fluctuations, fluctuation theorems, and counting statistics in quantum systems, *Rev. Mod. Phys.* **81**, 1665 (2009).
- [59] C. Jarzynski, Equalities and inequalities: Irreversibility and the second law of thermodynamics at the nanoscale, *Annu. Rev. Condens. Matter Phys.* **2**, 329 (2011).
- [60] For simplicity, the system and reservoir were assumed to be decoupled during protocol execution. However, in the proposed experiment, the bath remains coupled to the system throughout the process. Although there are subtleties when dealing with *strong-coupling* scenarios (see [77] and [78] for more and details) the Eq. (13) remains valid for both cases.
- [61] A. Ashkin, Acceleration and trapping of particles by radiation pressure, *Physical Review Letters* **24**, 156 (1970).
- [62] A. Ashkin, K. Schütze, J. Dziedzic, U. Euteneuer, and M. Schliwa, Force generation of organelle transport measured in vivo by an infrared laser trap, *Nature* **348**, 346 (1990).
- [63] S. M. Block, L. S. Goldstein, and B. J. Schnapp, Bead movement by single kinesin molecules studied with optical tweezers, *Nature* **348**, 348 (1990).
- [64] C. Bustamante, J. F. Marko, E. D. Siggia, and S. Smith, Entropic elasticity of  $\lambda$ -phage dna, *Science* **265**, 1599 (1994).
- [65] J. T. Finer, R. M. Simmons, and J. A. Spudich, Single myosin molecule mechanics: piconewton forces and nanometre steps, *Nature* **368**, 113 (1994).
- [66] C. Yi, C.-W. Li, S. Ji, and M. Yang, Microfluidics technology for manipulation and analysis of biological cells, *Analytica Chimica Acta* **560**, 1 (2006).
- [67] A. Bérut, A. Arakelyan, A. Petrosyan, S. Ciliberto, R. Dillenschneider, and E. Lutz, Experimental verification of landauer’s principle linking information and thermodynamics, *Nature* **483**, 187 (2012).
- [68] S. Toyabe, T. Sagawa, M. Ueda, E. Muneyuki, and M. Sano, Experimental demonstration of information-to-energy conversion and validation of the generalized jarzynski equality, *Nature Physics* **6**, 988 (2010).
- [69] T. T. Martins, *Studies of microscopic nonequilibrium stochastic dynamics in optical tweezers*.
- [70] J. A. Albay, G. Paneru, H. K. Pak, and Y. Jun, Optical tweezers as a mathematically driven spatio-temporal potential generator, *Optics express* **26**, 29906 (2018).
- [71] K. Berg-Sørensen and H. Flyvbjerg, Power spectrum analysis for optical tweezers, *Review of Scientific Instruments* **75**, 594 (2004), [https://pubs.aip.org/aip/rsi/article-pdf/75/3/594/19088275/594.1\\_online.pdf](https://pubs.aip.org/aip/rsi/article-pdf/75/3/594/19088275/594.1_online.pdf).
- [72] P. Welch, The use of fast fourier transform for the estimation of power spectra: a method based on time averaging over short, modified periodograms, *IEEE Transactions on audio and electroacoustics* **15**, 70 (1967).
- [73] While Eq. (27) is the standard method for calibrating optical tweezers, we use a fitting function that also takes into account hydrodynamic interactions and inertial effects, as detailed in [79]. According to [80], memory effects become significant for trap calibration at high sampling frequencies, making these corrections essential for accurate estimations of potential.
- [74] We do not use the derivative  $d\lambda/dt = \Delta\lambda/\tau_P$ ; instead, we compute it directly from the PD output signal.
- [75] C. Jarzynski, Rare events and the convergence of exponentially averaged work values, *Physical Review E* **73**, 046105 (2006).
- [76] The particle’s equilibrium position at constant intensity determines the amplification factor. Since the trapping beam intensity varies during the process, the amplification factor may change with the particle’s movement along the  $z$ -axis due to radiation pressure. However, without access to the actual dynam-

ics in this direction, the amplification factor is calculated based on the initial state, represented as  $S_x = S_{fit,x}(\langle V_{PD,eq} \rangle)$ , where  $\langle V_{PD,eq} \rangle$  is the average reading during the equilibrium period. For the short protocols, the particle's  $z$  position does not change significantly, making this approximation sufficient.

- [77] C. Jarzynski, Equalities and inequalities: Irreversibility and the second law of thermodynamics at the nanoscale, in *Time: Poincaré Seminar 2010*, edited by B. Duplantier (Springer Basel, Basel, 2013) pp. 145–172.
- [78] C. Jarzynski, Nonequilibrium work theorem for a system strongly coupled to a thermal environment, *Journal of Statistical Mechanics: Theory and Experiment* **2004**, P09005 (2004).
- [79] T. Franosch, M. Grimm, M. Belushkin, F. M. Mor, G. Foffi, L. Forró, and S. Jeney, Resonances arising from hydrodynamic memory in brownian motion, *Nature* **478**, 85 (2011).
- [80] B. Lukić, S. Jeney, Ž. Sviben, A. J. Kulik, E.-L. Florin, and L. Forró, Motion of a colloidal particle in an optical trap, *Physical Review E* **76**, 011112 (2007).